

Turgor – a limiting factor for radial growth in mature conifers along an elevational gradient

Richard L. Peters^{1,2,3} , Kathy Steppe³ , Henri E. Cuny^{1,4} , Dirk J.W. De Pauw³, David C. Frank^{1,5} , Marcus Schaub¹ , Cyrille B.K. Rathgeber⁶ , Antoine Cabon^{7,8}  and Patrick Fonti¹ 

¹Forest Dynamics, Swiss Federal Institute for Forest, Snow and Landscape Research (WSL), Zürcherstrasse 111, Birmensdorf CH-8903, Switzerland; ²Department of Environmental Sciences - Botany, Basel University, Schönbeinstrasse 6, Basel CH-4056, Switzerland; ³Laboratory of Plant Ecology, Department of Plants and Crops, Faculty of Bioscience Engineering, Ghent University, Coupure links 653, Ghent B-9000, Belgium; ⁴Institut National de l'Information Géographique et Forestière (IGN), 1 rue des blanches terres, Champigneulle 54115, France; ⁵Laboratory of Tree-Ring Research, 1215 E. Lowell Street, Tucson, AZ 8572, USA; ⁶Université de Lorraine, AgroParisTech, INRAE, Nancy, Silva 54000, France; ⁷Joint Research Unit CTFC - AGROTECNIO, Solsona E-25280, Spain; ⁸CREAF, Cerdanyola del Vallès, Barcelona E-08193, Spain

Summary

Author for correspondence
Richard L. Peters
Email: richard.peters@wsl.ch

Received: 2 June 2020
Accepted: 29 July 2020

New Phytologist (2021) 229: 213–229
doi: 10.1111/nph.16872

Key words: climate change, process-based model, radial stem growth, tree hydraulics, tree rings, wood formation.

- A valid representation of intra-annual wood formation processes in global vegetation models is vital for assessing climate change impacts on the forest carbon stock. Yet, wood formation is generally modelled with photosynthesis, despite mounting evidence that cambial activity is rather directly constrained by limiting environmental factors.
- Here, we apply a state-of-the-art turgor-driven growth model to simulate 4 yr of hourly stem radial increment from *Picea abies* (L.) Karst. and *Larix decidua* Mill. growing along an elevational gradient. For the first time, wood formation observations were used to validate weekly to annual stem radial increment simulations, while environmental measurements were used to assess the climatic constraints on turgor-driven growth.
- Model simulations matched the observed timing and dynamics of wood formation. Using the detailed model outputs, we identified a strict environmental regulation on stem growth (air temperature > 2°C and soil water potential > –0.6 MPa). Warmer and drier summers reduced the growth rate as a result of turgor limitation despite warmer temperatures being favourable for cambial activity.
- These findings suggest that turgor is a central driver of the forest carbon sink and should be considered in next-generation vegetation models, particularly in the context of global warming and increasing frequency of droughts.

Introduction

Wood formation plays a critical role within the terrestrial carbon cycle and its sensitivity to climate change will impact the Earth's climate system (Bonan, 2008; Pan *et al.*, 2011; Popkin, 2019). Projections of future forest carbon pools are usually provided by dynamic global vegetation models (DGVMs; Cox *et al.*, 2000; Sitch *et al.*, 2008), which are increasingly scrutinized for their ability to correctly represent the wood formation processes (De Kauwe *et al.*, 2014; Pugh *et al.*, 2016; Fatichi *et al.*, 2019; Friend *et al.*, 2019). In particular, the assumption that wood formation is mainly regulated by photosynthesis (i.e. carbon source limitation; Boisvenue & Running, 2006), is being criticized. Furthermore, such simulations show mismatches with tree ring-based biomass estimates and sensitivity of growth to climate variations (Tei *et al.*, 2017; Klesse *et al.*, 2018). Moreover, limited agreement has been found between above-ground biomass increment and carbon uptake derived from flux tower measurements (Babst *et al.*, 2014; Delpierre *et al.*, 2016; Pappas *et al.*, 2020). A

common explanation is that wood formation is not solely dependent on photoassimilate production, but also on limitations of the cambium to fix carbon (Fatichi *et al.*, 2014). Indeed, low temperatures and reduced water availability limit cambial activity at higher thresholds than photosynthesis (Körner, 2008; Parent *et al.*, 2010; Muller *et al.*, 2011; Rossi *et al.*, 2016). As a consequence, wood formation is expected to be more sink-limited under drier and colder environmental conditions than carbon assimilation. Our predictions of forest productivity are thus expected to improve by considering sink-limiting processes within DGVMs (Guillemot *et al.*, 2017; Huntzinger *et al.*, 2017).

Assimilated carbon is invested in woody stems to facilitate water and nutrient transport, mechanical support, and storage for carbohydrates, water and defence compounds (Kozłowski & Palardy, 1997; Fournier *et al.*, 2006). Our knowledge of wood formation (or xylogenesis) originates primarily from conifer studies, where *c.* 90% of the stem's xylem is composed of dead wood cells, which are progressively formed via cell division by the

cambium (the vascular meristem) differentiated through cell enlargement, secondary cell wall formation and lignification, and finally matured through programmed cell death (Rathgeber *et al.*, 2016). Annual xylem radius increase (or tree rings) therefore depends on the number of cells produced by cambial division and their ability to enlarge under given environmental conditions (Cuny *et al.*, 2014). The relationships between climate and sub-annual wood formation observations are thus increasingly studied (Rossi *et al.*, 2016; Cuny *et al.*, 2019), providing valuable insights into the timing of wood formation and woody biomass production (Cuny *et al.*, 2015). Tree rings are forged through the interplay between climate and mechanisms impacting cambial activity (Cuny & Rathgeber, 2016), which involves carbon (Hölttä *et al.*, 2010) and nutrient availability (Norby *et al.*, 2010), internal hormonal signalling (Drew *et al.*, 2010; Hartmann *et al.*, 2017), temperature-dependent enzymatic kinetics (Parent *et al.*, 2010), and water-driven turgor pressure in the xylem (Steppe *et al.*, 2006; Steppe *et al.*, 2015). Yet, further model development is needed to incorporate relevant mechanisms underlying wood formation and its interaction with climate (but see Leuzinger *et al.*, 2013 and Guillemot *et al.*, 2017; Friend *et al.*, 2019).

Turgor pressure in forming xylem cells has been advanced as a central 'sink limiter' (Fatichi *et al.*, 2014; Steppe *et al.*, 2015), determining the initiation and rate of cell enlargement (Lockhart, 1965; Cosgrove, 1986; Steppe *et al.*, 2006). This is supported by experimental evidence, revealing a strict downregulation of growth during drought stress compared with photosynthetic activity (Muller *et al.*, 2011). Although cell division and enlargement are driven by hormones (Hartmann *et al.*, 2017), turgor above a 'yield' threshold provides the mechanical force for cell wall relaxation and subsequent cell enlargement (Génard *et al.*, 2001). A recent modelling study applied this paradigm on *Pinus sylvestris*, revealing the importance of turgor (regulated by soil water availability) in dictating the final tracheid diameter (Cabon *et al.*, 2020a), which raises the question about the relevance of this process in controlling overall radial growth rates.

Mechanistic models that aim to simulate intra-daily stem growth (of both xylem and phloem) focus on internal stem hydraulics (Steppe *et al.*, 2006; Génard *et al.*, 2008; De Swaef & Steppe, 2010; Hölttä *et al.*, 2010; De Schepper & Steppe, 2010; Nikinmaa *et al.*, 2014; Baert *et al.*, 2015; Salomón *et al.*, 2017, 2019). However, often these models have only been tested for short periods of up to a few months, are applied on young plants growing under controlled conditions, have a large multitude of parameters and require subdaily physiological measurements (Babst *et al.*, 2018). Moreover, although these models and other empirical approaches (e.g. Mencuccini *et al.*, 2017) allow researchers, to some extent, to disentangle daily irreversible stem growth patterns from bark water content changes, they have rarely been validated with independent measurements (i.e. measurements not used for model calibration) of wood formation (e.g. xylogenesis; Cuny *et al.*, 2019). There is thus a need to validate whether turgor pressure remains the crucial mechanism in regulating whole-tree radial growth on inter- and intra-annual timescales (Fonti & Jansen, 2012; Steppe *et al.*, 2015; Zuidema *et al.*, 2018).

Environmental conditions can severely limit carbon sink and source activity, yet with different sensitivities, as highlighted by Fatichi *et al.* (2014). For example, stem water potential changes within plants (i.e. induced by drought) affect turgor pressure and cell expansion rates, and strongly inhibit cambial activity below -1 MPa (Muller *et al.*, 2011; Cabon *et al.*, 2020a), while at similar water status the conductance of water and photosynthetic activity are less affected (Tardieu *et al.*, 2011). Similarly, cambial activity shows a highly consistent response to varying temperature which can be explained by the effect of temperature on metabolic activity (Parent *et al.*, 2010; Parent & Tardieu, 2012), where temperatures $< 5^{\circ}\text{C}$ have been shown to prohibit cambial activity (Rossi *et al.*, 2016; Cabon *et al.*, 2020b). Besides the limited efforts in quantifying such environmental thresholds on mature trees, the question remains as to what extent turgor limitation hampers inter- and intra-annual radial stem growth with future increasing temperatures, rising vapour pressure deficit and decreasing water availability (Ciais *et al.*, 2005; Grossiord *et al.*, 2020). In particular, forests growing at high elevations and latitudes have been identified as hotspots of change (e.g. Peters *et al.*, 2017; Babst *et al.*, 2019), although it has to be established where and when the benefit of relieving temperature limitation will be outweighed by increasing drought stress. Disentangling these limiting variables along steep thermal and soil moisture gradients, as present in mountainous ecosystems (i.e. a space-for-time experimental setting; Moser *et al.*, 2009), will thus provide insights into both environmental thresholds of growth mechanisms and their future role with persistent environmental warming.

In this study, we rely on a turgor-driven mechanistic model (originating from Steppe *et al.*, 2006 and De Schepper & Steppe, 2010) to simulate growth of *Larix decidua* Mill. and *Picea abies* (L.) Karst. trees along an elevational gradient in the Central Swiss Alps (from 1300 to 2200 m asl) and at contrasting wet and dry site conditions (see Peters *et al.*, 2019). We used a unique multi-annual dataset of subhourly sap flow and stem radius variation as model input and calibration data, respectively, while using weekly to annual radial xylem growth observations of trees for independent validation (Cuny *et al.*, 2019). We specifically addressed three hypotheses: (1) inter- and intra-annual radial wood formation in both species can be explained by turgor-driven radial growth; (2) turgor-driven growth rates show a stronger environmental regulation than conductance of water, because photosynthesis persists when growth is already inhibited; and (3) turgor limitation will become more prevalent with warming, compared with the relief of temperature limitation in high-elevation forests. The latter is tested by analysing the dynamics of turgor limitation to warmer site conditions (i.e. at lower elevations), while considering temperature-dependent enzymatic kinetics, which increase cell wall relaxation at higher temperatures (Parent *et al.*, 2010).

Materials and Methods

Study design and allometric measurements

The study was performed on trees growing at five sites in the Swiss Alps (Lötschental, $46^{\circ}23'40''\text{N}$, $7^{\circ}45'35''\text{E}$; Fig. 1a),

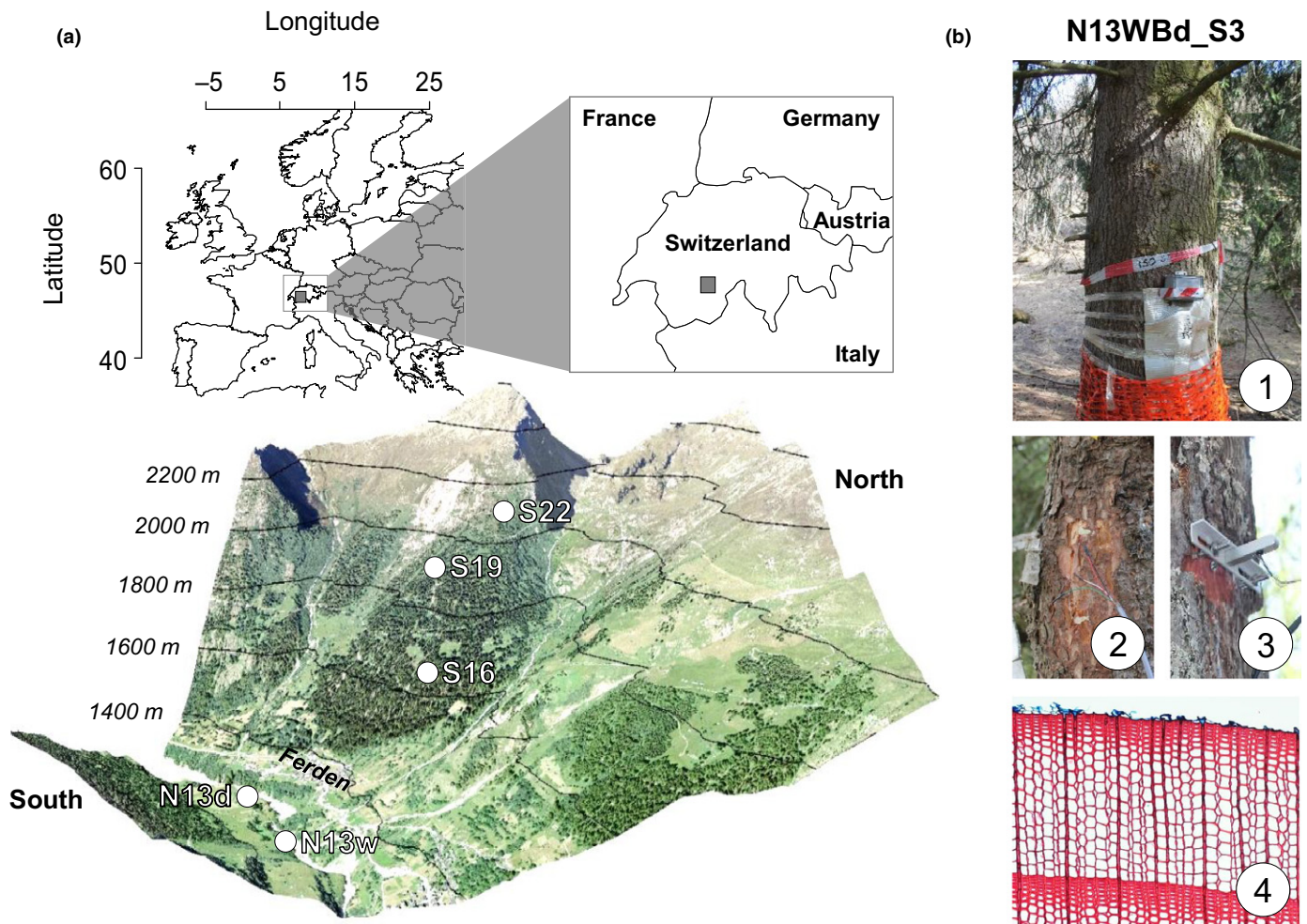


Fig. 1 Research sites and experimental setup. (a) In the Swiss Lötschental, at every 300 m asl, a site was established (e.g. 2200 m asl = 22) on either the north- N) or south-facing S) slope (top left panel). At the valley bottom, an additional site provides contrast in soil water availability (dry = N13d and wet = N13w). (b) At each site two to three trees per species were continuously monitored from 2012 to 2015. Picture 1 provides an example of a mature *Picea abies* tree which was monitored at the N13w site (N13WBd_S3 in Table 1). Each tree was equipped with a thermal dissipation probe sap flow sensor (picture 2) and point dendrometer (picture 3), which were used as model input and calibration, respectively. Model simulations were validated against independent measurements of xylem diameter growth, constructed with weekly wood formation observations and anatomical properties (picture 4).

including European larch (*Larix decidua* Mill.) and Norway spruce (*Picea abies* (L.) Karts.). Four sites were distributed along an elevational gradient (at c. 1300, 1600, 1900 and 2200 m asl) from the valley bottom to the treeline, in addition to a site with wet soil conditions at the valley bottom. The mean growing season temperature decreases by 3.2°C when moving from the valley bottom up to the treeline (see Supporting Information Fig. S1; Peters *et al.*, 2019). A total of 20 trees of both species were selected (two to three trees per site and species, with only *L. decidua* at 2200 m asl; Table 1) for continuous high-resolution physiological monitoring over 4 yr (2012–2015; 11 *L. decidua* and nine *P. abies*; Fig. 1b). Additionally, four trees per site and species were selected for 2 yr (2012–2013) for weekly monitoring of wood formation (as described in Cuny *et al.*, 2019).

Allometric properties were collected from all monitored trees on which physiological monitoring was performed (see Cuny *et al.*, 2019 for allometric properties of trees on which wood formation monitoring was performed). Allometric measurements

included: stem diameter at breast height (DBH, cm); tree height (m); stem length up to the crown base (l_{stem} , m; Vertex, Haglöf, Sweden); sapwood (T_{sapwood} , cm) and heartwood thickness (r_{hw} , cm) (measured from two increment cores taken perpendicular to the slope, using an increment borer; Haglöf, Sweden; see Peters *et al.*, 2017); and bark (T_{bark} , cm) and phloem thickness (T_{phloem} , cm) (using a Trephor puncher; Tesaf, University of Padova, Italy) at breast height (1.3 m above ground).

Physiological monitoring and meteorological data

On each tree stem we performed continuous hourly measurements of stem radius (r_{stem} , μm) using a high-precision point dendrometer installed onto the outer bark (King *et al.*, 2013; Ecomatik model DR, Munich, Germany) and sap flux density (F_d , $\text{cm}^3 \text{m}^{-2} \text{h}^{-1}$) using thermal dissipation probes (Peters *et al.*, 2019; Tesaf, University of Padova, Italy; Fig. 1b). Both sap flow and dendrometer sensors were installed at the slope-facing

Table 1 Characteristics of the monitored trees and the applied model calibration procedure.

Elevation (m asl)	Site code	Species	Tree	DBH (cm)	l_{stem} (m)	T_{phloem} (cm)	T_{bark} (cm)	T_{sapwood} (cm)	Age (yr)	Cal. 2015	Cal. MW
1300 (dry)	N13d	<i>Larix decidua</i>	N13Bd_L1	29.5	7.2	0.46	2.88	1.5	131	X	X
			N13Bd_L2	32.0	10	0.36	2.23	1.8	128	X	X
		<i>Picea abies</i>	N13Ad_S1	30.7	2.8	0.48	0.68	2.5	90	X	X
			N13Ad_S2	48.1	2.9	0.33	1.10	5.3	93	X	X
1300 (wet)	N13w	<i>Larix decidua</i>	N13WAd_L1	78.0	8.2	0.80	4.35	2.2	148	X	X
			N13WBd_L2	89.3	8.8	0.83	7.90	2.4	164	X	X
			N13WBd_L3	52.0	5.6	0.37	4.90	2.4	134	X	X
		<i>Picea abies</i>	N13WAd_S1	81.0	3.1	0.66	2.60	9.1	85	X	X
			N13WAd_S2	62.8	5.8	0.63	1.30	6.9	81	X	X
			N13WBd_S3	80.7	4.4	0.71	1.75	9.0	109	X	X
1600	S16	<i>Larix decidua</i>	S16Bd_L1	75.2	15	0.40	7.05	3.5	371		X
			S16Ad_L1	38.5	13	0.39	2.75	2.6	69		X
		<i>Picea abies</i>	S16Ad_S2	38.2	6.7	0.74	1.50	4.2	62		X
			S16Bd_S2	56.2	13	0.53	2.00	2	461		X
1900	S19	<i>Larix decidua</i>	S19Ad_L1*	48.0	5.3	0.28	7.35	3.2	200		
			S19Bd_L1	48.7	9.8	0.51	4.60	1.8	326		X
		<i>Picea abies</i>	S19Ad_S2	34.1	8.8	0.62	1.25	1.7	137		X
			S19Bd_S2	47.5	5.5	0.29	1.45	5.5	229		X
2200	S22	<i>Larix decidua</i>	S22Ad_L1	47.0	8.9	0.59	2.95	2.4	269	X	X
			S22Ad_L2	55.7	5.5	0.45	4.10	3.1	280	X	X

For each individual the diameter at breast height (DBH), stem length (l_{stem}), thickness of the bark (T_{bark}), phloem tissue (T_{phloem}) and sapwood (T_{sapwood}), and age are provided. Two calibration procedures were applied, including the 2015 weekly calibration using branch water potential (ψ_{leaf}) measurements (Cal. 2015) to constrain parameters, and the moving-window calibration over the entire growing season (Cal. MW). The tree labels match previously published work (see Peters *et al.*, 2018, 2019).

side of each stem at *c.* 1.6 m above ground (Fig. 1). The F_d was calculated using the method described in Peters *et al.* (2018), applying a species-specific calibration, dampening correction and environmental dependent zero-flow conditions. Needed as input for the model, F_d was multiplied by sapwood area to obtain water flow to the crown (F_{crown} , g h^{-1}). The initial diameter of the stem (D_{stem} (cm) = $r_{\text{stem}} \times 2$, required for model calibration) was calculated from the tree diameter considering xylem and phloem ($\text{DBH} - T_{\text{bark}} \times 2 + T_{\text{phloem}} \times 2$).

For improving model calibration, branch water potential (a proxy for leaf water potential; ψ_{leaf} , MPa) measurements were taken at N13d, N13w and S22 during four diurnal campaigns (2 h interval from 05:00 to 21:00 h CET on 19 April 2014, 27 May 2015, 21 July 2015 and 24 September 2015) and weekly sampling at midday (11:00–15:00 h CET) was performed during the 2015 growing season. Measurements were performed using a Scholander pressure chamber (Boyer, 1967) on four twigs (*c.* 5 cm) per tree. During the diurnal campaigns, additional twigs were covered with aluminium foil, 2 h before sampling (Begg & Turner, 1970) to determine stem water potential (ψ_{stem} , MPa).

For independent model validation, interannual growth was established for the monitored trees by measuring tree-ring width (mm) using an increment borer in 2015 close to the dendrometer sensor. Wood formation was determined by collecting weekly microcores from 2012 to 2013 (from May to November) to produce thin sections for counting the number of cambial, enlarging, wall-thickening and mature cells (see Cuny *et al.*, 2019 for details on sample processing). These data were combined with wood anatomical properties of the corresponding completed ring to

determine radial xylem growth (r_{xy}) according to Cuny *et al.* (2014). In short, digital images of the corresponding tree-ring thin sections were analysed using image analysis software (ROXAS; von Arx & Carrer, 2014) to measure the dimensions of tracheids along radial files. Then, RAPTOR (Peters *et al.*, 2017) was used to establish tracheid dimensions along an average of 30 radial files.

At each site, micrometeorological conditions were monitored, including 15 min resolved air temperature (T_a , °C) and relative humidity (RH, %; U23-002 Pro; Onset, MA, USA; also used to calculate vapour pressure deficit or D (kPa); see WMO, 2008), as well as hourly soil water potential measurements at 10 and 70 cm depth (ψ_{soil} , MPa; Decagon, USA, MPS-2). Maximum ψ_{soil} across both depths was used, assuming roots had equal access to water across the soil profile. Hourly global radiation (R_g , W m^{-2}) was measured at N13d using a microstation (H21-002 Micro Station; Onset) and pyranometer (S-LIB-M003; Onset) (see Peters *et al.* (2019) for a detailed description of the processing of the micrometeorological data).

Turgor-driven growth model

This study makes use of a mechanistic model consisting of a water transport (Fig. 2a) and stem diameter (Fig. 2b) module, using equations detailed in Steppe *et al.* (2006) and De Schepper & Steppe (2010), assuming that growth is solely limited by sink activity (i.e. turgor-driven cell expansion). The model requires information on tree-specific allometric characteristics, hourly tree physiological measurements and micrometeorological data and parameters, to disentangle reversible (i.e. daily shrinkage and

swelling as a result of water transport) from irreversible (i.e. wood formation) diameter growth. In addition to applying this model containing solely hydraulic mechanisms affecting growth, we applied a second modelling approach which incorporates temperature-dependent enzymatic kinetics affecting cell wall extensibility to assess the importance of temperature vs turgor limiting growth. The model was validated against independent weekly to annual wood formation observations.

The turgor-driven growth model (Fig. 2) simulates water exchange between stem compartments induced by sap flow,

which allows differences in water potentials between compartments to be assessed. The model considers three compartments, including the roots, stem (trunk of the tree until the crown base) and crown (Fig. 2c). The stem is modelled by three coaxial cylinders, including heartwood, water-conducting sapwood and an elastic stem storage compartment (consisting of cambium and phloem tissue) but excluding inactive bark. Water transport from the roots through the sapwood (F_{stem} , $g\ h^{-1}$) is determined by the difference between root water potential (ψ_{root} , MPa) and ψ_{stem} divided by the hydraulic resistance of the xylem (R_x ,

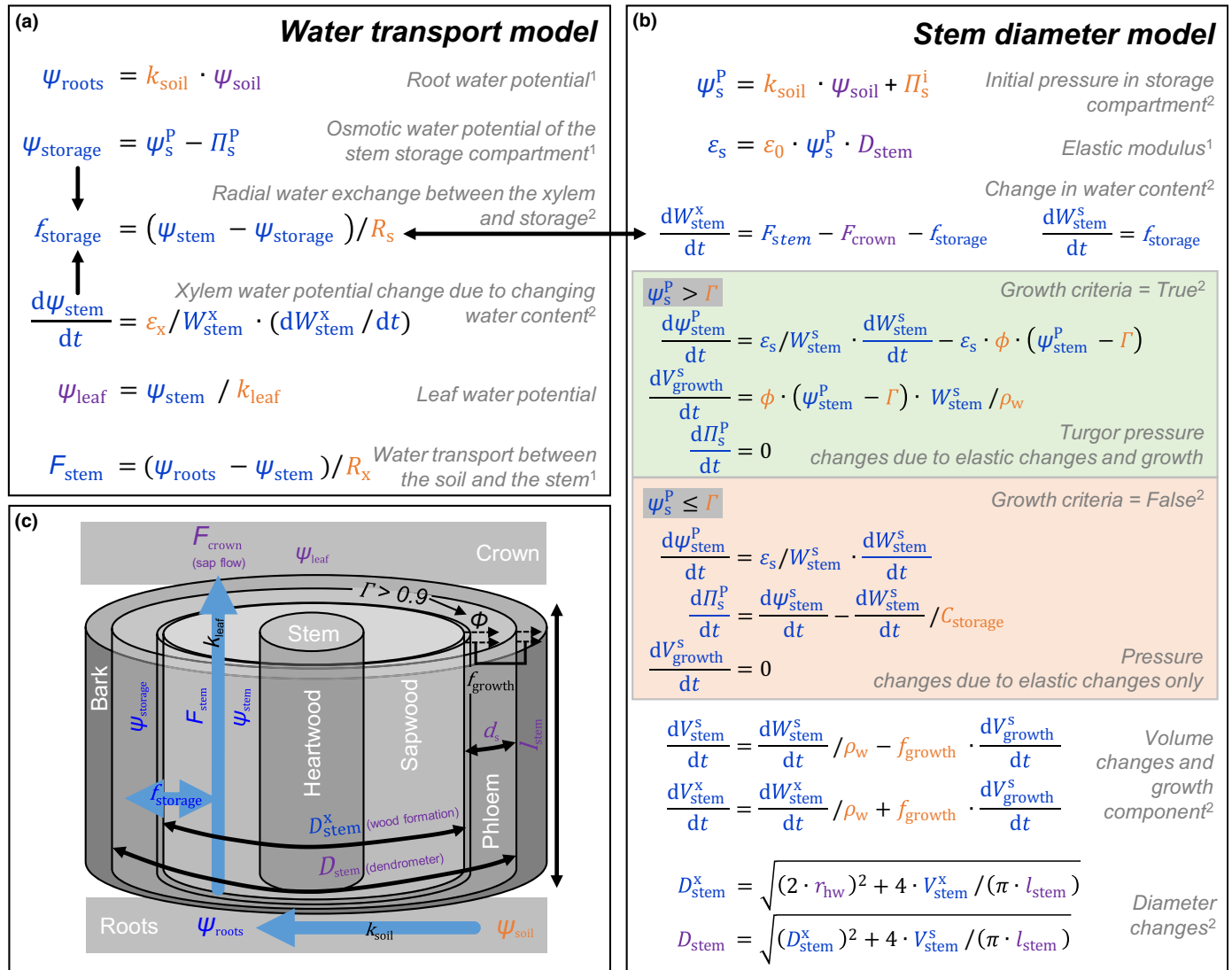


Fig. 2 Scheme of water transport and stem diameter model linking sap flow dynamics, dendrometer measurements and growth. (a) The water transport model assesses tree-internal flows when water moves from the soil to the atmosphere. Water flow is driven by transpiration (F_{crown}) and utilizes either water moving from the soil (F_{stem}) or from the storage compartment ($f_{storage}$). (b) The water transport model steers the stem diameter model by impacting the pressure ($\psi_{storage}$) and turgidity (ψ_s^p) of the storage compartment which consequently changes the outer stem diameter (D_{stem}). Reversible growth is determined by the elasticity of the storage and xylem tissue, while irreversible diameter change or xylem growth (D_{stem}^x) occurs when turgor in the forming tissues exceeds a threshold (Lockhart, 1965; Steppe *et al.*, 2006). (c) Graphical representation of the stem compartment. The model includes four tissues, where nonfunctional bark and heartwood are hydraulically inactive, while the sapwood and the phloem (considered as the storage compartment, including the cambium) facilitate water transport and store water, respectively. The origin of the equations is highlighted by the '1' and '2' superscripts, referring to Steppe *et al.*, (2006) and De Schepper & Steppe (2010), respectively. The colours indicate whether the symbol shows a derived variable (in blue), a parameter (in orange) or a physiological/environmental measurement (in purple). A description of all variables and parameters used by the model is given in Table 2.

MPa h g⁻¹; see Table 2). Moreover, the simulated Ψ_{stem} was used to calculate Ψ_{leaf} by using a proportional constant derived from the *in situ* leaf and stem water potential measurements (k_{leaf} ; Table S1). The imbalance between F_{stem} and water transported to the crown (F_{crown} , g h⁻¹; sap flow measurements) defines the amount of water that is used from the storage compartment (f_{storage}) and is calculated using the resistance for radial water transport (R_s , MPa h g⁻¹) and the capacitance of the tissue to release water (C_{storage} , g MPa⁻¹). Thus, the model estimates the storage water potential (ψ_{storage} , MPa) and subsequently the volume of water in the storage compartment (V_{stem}^s , m³). Depending on a fixed initial osmotic potential (Π_s^i , MPa; assuming no carbon limitation), these dynamics are used to determine turgor pressure in the storage compartment (ψ_s^p , MPa). Daily reversible fluctuations in D_{stem} (as seen in dendrometer measurements) are determined by pressure changes in sapwood (affected by its elastic modulus: e_x , MPa) and storage compartment (determined by the storage compartment's elastic modulus: e_s , MPa) using Hooke's law (De Schepper & Steppe, 2010). The dynamics of ψ_s^p are used to calculate irreversible diameter growth (D_{stem}^x). Growth occurs when ψ_s^p exceeds a threshold value for cell wall yielding (Γ , MPa; Lockhart, 1965; Steppe *et al.*, 2006), which increases both the dimensions of the phloem and the xylem compartment (whose fractional investment is defined by f_{growth}). The increase in irreversible radial growth as a result of ψ_s^p exceeding Γ depends on the extensibility of cell walls (ϕ), which is a fixed parameter for the initial modelling scenario.

The second modelling approach assessed the impact of temperature-dependent enzymatic kinetics on ϕ (Eqn 1). We hypothesize that cell wall extensibility is increased or decreased, with high vs low temperatures, respectively, as a result of the effect of temperature on enzymatic kinetics, which drive the release of cellulose microfibrils (Cosgrove, 2000). A combination of the Eyring (2004) equation, expressing the enzymatic reaction rate with T_a (expressed in K), with the equation of the rate of reversible denaturation of enzymes provides the framework for expressing enzymatic kinetics as a function of temperature (Johnson *et al.*, 1942; Parent *et al.*, 2010).

$$F(T) = \frac{AT_a e^{\left(\frac{-\Delta H_A^\ddagger}{RT_a}\right)}}{1 + e^{\left[\frac{\Delta S_D}{R} \left(1 - \frac{\Delta H_D}{\Delta S_D T_a}\right)\right]}} \quad \text{Eqn 1}$$

where $F(T)$ (unitless) is considered the reaction rate, where ΔH_A^\ddagger [kJ mol⁻¹] is the enthalpy of activation (affecting the curvilinear of the increasing part of the function), R (J K⁻¹ mol⁻¹) is the gas constant, and A (unitless) is a scaling constant. Denaturation of enzymes (denominator) is determined by enthalpy (ΔH_D , kJ mol⁻¹) and entropy (ΔS_D , kJ mol⁻¹ K⁻¹) between the catalytically active and inactive states of the enzymes. In addition, to comply with the observation made by Körner (2003), we set $F(T) = 0$ when $T_a < 5^\circ\text{C}$. Parameters were selected according to Parent *et al.* (2010), where $\Delta H_A^\ddagger = 87.5$ kJ mol⁻¹, $\Delta H_D = 333$ kJ mol⁻¹, and $\Delta S_D = 1.09$ kJ mol⁻¹ K⁻¹. The function is scaled using $A = 15.168 \times 10^{10}$, to scale the response

function to have a ϕ of 0.006 MPa⁻¹ h⁻¹ (Table S1) at 15°C (approximate night-time temperature during the growing season).

Modelling and statistical analyses

Model parameters were established with existing literature and tree-specific measurements (see Table S1 and associated Figs S2–S5 and Tables S2–S4). Model calibrations, simulations and sensitivity analyses were performed using PHYTO-SIM (v.2.1, Phyto-IT, Gent, Belgium; see Notes S1 for details and associated Fig. S6) on each individual tree. Two types of model calibrations were used for different subsets of trees, namely the 2015 and moving-window calibration (Table 1). First calibrations were performed for the measurements in 2015 for 7 d periods when ψ_{leaf} was measured (at N13d, N13w and S22). These weekly calibrations were performed to analyse the behaviour of hydraulic parameters (R_x , C_{storage} , Π_s^i and R_s ; Table S5). Additionally, as ψ_{leaf} measurements were not available for all years, we performed analyses to test model performance with C_{storage} or R_x , as a fixed parameter (Notes S2 and associated Figs S7, S8 and Tables S5, S6). After constraining C_{storage} and Π_s^i , a 7 d moving-window calibration was applied to dendrometer measurements of all trees and years to obtain approximate hourly D_{stem}^x dynamics. The growing-season calibrations were run from 2012 to 2015 with fixed C_{storage} (dependent on storage compartment volume) and Π_s^i (c. 1.3 MPa). The calibrations (of R_x and R_s) were performed with a 7 d moving-window approach from May to August. The moving window shifts forward while providing a 3 d overlap with the previous calibration (to prevent spurious end effects of the simulated parameters), using both initial conditions and parameters (of R_s and R_x) from the previous calibration. To test Hypothesis 1, simulated daily growth patterns were averaged over a 7 d moving window of daily growth patterns (e.g. Fig. S9) and compared with the weekly wood formation observations (Fig. S10) and ring width.

To test Hypothesis 2, we assessed the environmental response of turgor-driven radial growth (mm d⁻¹) by relating daily growth rates to daily mean T_a and ψ_{soil} . Additionally, the environmental response of crown conductance (g_c , g_{water} m⁻² sapwood s⁻¹ kPa⁻¹) was analysed according to Meinzer *et al.*, (2013). In short, daily mean g_c was determined with the ratio of F_d to D under conditions of negligible stem capacitance. We calculated g_c every 15 min and excluded measurements where R_g was < 500 W m⁻² to avoid stem capacitance effects on sap flow and transpiration during dawn and dusk (see Peters *et al.*, 2019 for a more detailed description). To account for collinear environmental factors, we analysed T_a when removing all data with a $\psi_{\text{soil}} < -0.2$ MPa, while for ψ_{soil} we removed all T_a data < 11°C. The fraction of days over the total number of days analysed where growth and g_c exceeded a given threshold was calculated to assess the probability of growth and g_c occurring under specific environmental conditions (> 2.5 $\mu\text{m d}^{-1}$ for radial growth and > 15 g m⁻² s⁻¹ kPa⁻¹ for g_c). The threshold values were determined after visual inspection

Table 2 Symbol, unit, and description of the model parameters, monitoring data, algebraic variables and derived variables.

Type	Symbol	Unit	Description	
Parameters	ρ_w	g m^{-3}	Density of water	
	l_{stem}	m	Length of the stem	
	D_{stem}^1	m	Initial diameter of the outer diameter of the stem segment (DBH)	
	d_s	m	Initial thickness of the stem storage compartment	
	r_{hw}	m	Radius of the nonconductive xylem (heartwood)	
	C_{storage}^*	g MPa^{-1}	Capacitance of the stem storage compartment	
	R_x^*	MPa h g^{-1}	Flow resistance in the stem compartment of the active xylem (sapwood)	
	R_s^*	MPa h g^{-1}	Exchange resistance between the active xylem of the stem and the storage compartment (bark)	
	Π_s^*	MPa	Initial osmotic pressure of living tissue of the stem	
	f_{water}	Unitless	Water fraction of the stem compartment	
	k_{leaf}	Unitless	Proportionality constant for calculating ψ_{stem}	
	o	m^{-1}	Proportionality constant	
	x	MPa	Elastic modulus of the xylem	
	ϕ	$\text{MPa}^{-1} \text{h}^{-1}$	Extensibility of cell walls in relation to nonreversible dimensional changes (radial wood growth)	
	Γ	MPa	Threshold turgor pressure	
	f_{growth}	Unitless	Fraction of growth contributing to xylem formation	
	ψ_{soil}^1	MPa	Initial soil water potential	
	k_{soil}	Unitless	Proportionality constant for calculating ψ_{roots}	
	T_{phloem}	cm	Thickness of the visually distinguishable phloem (assumed to equal d_s)	
	T_{bark}	cm	Overall thickness of the bark of the stem	
	T_{sapwood}	cm	Thickness of the visually distinctive sapwood	
	ΔH_A^1	kJ mol^{-1}	Enthalpy of activation	
	R	$\text{J K}^{-1} \text{mol}^{-1}$	Gas constant	
	A	Unitless	Scaling constant	
	ΔH_D	kJ mol^{-1}	Denaturation of enzymes by enthalpy between the catalytically active and inactive states of the enzymes	
	ΔS_D	$\text{kJ mol}^{-1} \text{K}^{-1}$	Denaturation of enzymes by entropy between the catalytically active and inactive states of the enzymes	
	Monitoring data	F_{crown}	g h^{-1}	Water flow from the stem xylem towards the crown compartment (obtained from F_d)
		F_d	$\text{cm}^3 \text{m}^{-2} \text{h}^{-1}$	Measurement of sap flux density using thermal dissipation probes
		D_{stem}	m	Over bark diameter (obtained from r_{stem})
		r_{stem}	μm	Dendrometer measurement of the stem radius
		r_{xyl}	μm	Radius of the xylem (obtained from xylogensis observations)
		ψ_{leaf}	MPa	Leaf water potential (measurements)
ψ_{soil}		MPa	Soil water potential (measurements)	
R_g		W m^{-2}	Global radiation	
RH		%	Relative air humidity	
T_a		$^{\circ}\text{C}$	Air temperature	
Algebraic variables		f_{stem}	g h^{-1}	Water exchange between the xylem and the storage compartment
		F_{stem}	g h^{-1}	Water flow from the roots towards the stem xylem compartment
	D_{stem}^x	m	Xylem diameter of the stem segment	
	D_{stem}	m	Outer diameter of the stem	
	ϵ_s	MPa	Bulk elastic modulus of living tissue in relation to reversible dimensional changes	
	ψ_{roots}	MPa	Root water potential	
	ψ_{storage}	MPa	Water potential in the storage compartment	
	ψ_{stem}	MPa	Stem water potential	
	D	kPa	Vapour pressure deficit	
	$F(T)$	Unitless	Enzymatic reaction rate affecting ϕ	
	g_c	$\text{g m}^{-2} \text{s}^{-1} \text{kPa}^{-1}$	Crown conductance	
	Derived variables	W_{stem}^x	g	Water content in the stem xylem compartment
		W_{stem}^s	g	Water content in the stem storage compartment
		ψ_{stem}^p	MPa	Pressure component of the xylem water potential
		ψ_{stem}^s	MPa	Pressure component of the water potential in the storage compartment
V_{stem}^x		m^3	Volume of the xylem stem tissue	
V_{stem}^s		m^3	Volume of the stem storage compartment	
V_{growth}^s		m^3	Growth volume for the entire stem	
Π_s^p		MPa	Osmotic component of the water potential in the storage compartment	

Symbols highlighted with an asterisk (*) were considered for the mechanistic model calibration.

of the output, as lower values are probably generated by measurement uncertainties in the model input data (i.e. sap flow measurements).

Finally, to test Hypothesis 3, a model calibration was performed where ϕ was made dependent on T_a to quantify the hours of turgor and temperature limitation across the gradient.

Statistical analysis of the comparison between model output (i.e. independent variable) and validation data (i.e. dependent variable) was performed with linear mixed-effect models (considering the site and nested individual as random factors for the intra-annual validation and solely the site as a random factor for the interannual analyses owing the low number of years, using the NLME package; Pinheiro *et al.*, 2020). Data-processing and statistical analyses of the comparison between model output and validation data were performed with R (v.3.2.00; R Core Team, 2013).

Results

Model parameterization and testing

The mechanistic model, simulating stem hydraulics, provided stem-diameter variations that fitted well with the observations of both growth and nongrowth periods (Fig. 3). Model calibrations and outputs revealed that parameters, such as hydraulic capacitance of the storage compartment (C_{storage}) and hydraulic resistance in the xylem (R_x), fell within realistic ranges, where R_x changed with elevation and species (e.g. R_x significantly increased under persistent drought conditions; Notes S2). This performance of the model was reflected in the high goodness of fit between D_{stem} and dendrometer measurements across sites and species for the calibration used to study the behaviours of hydraulic parameters (Table 3). Using hourly soil water potential (ψ_{soil}) and sap flow (F_{crown}) measurements as input, the model was able to estimate water potential and flows along the different environmental (soil and atmosphere) and tree (crown, stem xylem and bark storage) components and assess the turgor pressure (ψ_s^p) experienced by the cambial cells (Fig. 3). Growth (irreversible cell enlargement) of wood (D_{stem}^x) occurs when ψ_s^p exceeds a threshold for cell wall-yielding (Γ). This is mainly reached during night periods as shown in Fig. 3. The model parameters were calibrated for each individual tree growing at three sites (a wet and dry site at 1300 m asl and the treeline site at 2200 m asl; Notes S2), where weekly midday leaf water potential measurements were performed during the growing season of 2015 (ψ_{leaf}).

Validation of radial growth simulations against observations

Simulated wood radial growth (r_{xyl} derived from D_{xyl}) for each tree and week, during the growing season 2012–2015, was compared with observations of radial wood formation (Fig. 4). Simulated daily xylem growth rates (weekly-averaged) showed a considerable agreement with xylogenesis observations for 2012 and 2013 (Fig. 4a), especially for *L. decidua* at the treeline ($R^2 = 0.89$, $P < 0.0001$; Table 4). The goodness of fit decreases with elevation, with the larger deviation at the dry site in the valley bottom for 2013 (*P. abies*, $R^2 = 0.14$, $P = 0.112$; *L. decidua*, $R^2 = 0.21$, $P = 0.04$). On average, the goodness of fit was lower for *P. abies* than for *L. decidua* ($R^2 = 0.52$ and 0.70 , respectively), yet the seasonal patterns were generally well captured.

The largest deviations were detected at the end of the growing season, where simulated growth stopped earlier than observations at the valley bottom with dry conditions during 2013 (Fig. 4a). A comparison of simulated annual growth vs measured ring width from 2012 to 2015 showed a good agreement across sites and species (Fig. 4b). The slope of 0.89 ($P < 0.0001$, $n = 76$; with the site as a random factor) indicates that the model simulations slightly overestimate ring width. The 95% Bayesian credible interval indicates an overall uncertainty of *c.* 1 mm for modelled growth. For the moving-window calibrations, consistent patterns were found for R_s and R_x , with higher values at the start and end of the growing season and under drier conditions (Fig. S11).

Environmental regulation of growth and conductance

Simulated daily growth rates and crown conductance (g_c) were related to measurements of atmospheric temperature (T_a) and soil water potential (ψ_{soil}) in order to assess environmental conditions that regulate growth v and crown conductance (Fig. 5). Daily T_a at the sites along the gradient ranged from *c.* 0 to 20°C for June–August, while in the valley bottom the wet and dry site ψ_{soil} values ranged from *c.* 0 to –1.2 MPa (with the other sites only ranging up to *c.* –0.5 MPa, and decreasing drought severity with increasing elevation). These conditions fall into the range where offsets between photosynthetic activity and growth would be expected (Fig. 5a). Below 2°C, the probability of modelled growth to occur is only 23% (Fig. 5b), whereas the active crown conductance below this threshold is 43% (Fig. 5c). Note that daily growth rates increased up to 11°C, after which it stabilized and slowly decreased as a result of the increase in vapour pressure deficit (D in Fig. S8). The probability of growth decreased from 65% to 29% between –0.2 and –0.6 MPa ψ_{soil} , while almost no growth occurred below –0.6 MPa (Fig. 5b). Yet, g_c appeared to show a less steep decrease with decreasing ψ_{soil} , where sap flow still occurred at –1.2 MPa (Fig. 5c).

When incorporating temperature dependency of enzymatic kinetics affecting ϕ , simulations revealed that ϕ became less limiting with higher summer temperatures ($P < 0.0001$; –35 h °C^{–1} for summer or –50 h °C^{–1} when considering the growing season, 1 May to 1 October; $P = 0.0073$ with the site as a random factor; Fig. 6). Yet, with increasing summer temperatures, ψ_s^p became twice as limiting compared with relieving temperature limitation on ϕ (Fig. 6), with a 74 h increase in ψ_s^p limitation per 1°C increase in summer T_a (or 147 h °C^{–1} in the growing season). Although wet site conditions reduced this limitation (wet vs dry valley bottom site, $\Delta 431$ h ψ_s^p limitation; $P = 0.0001$), the trend of increasing time (h) of ψ_s^p limitation with increasing summer T_a remained (wet valley bottom site = 100 h ψ_s^p limitation °C^{–1}). However, note that this trend is less evident for the dry valley bottom site.

Discussion

For the first time, we present a multiannual validation of turgor dynamics in radial stem growth modelling for mature conifers growing under natural environmental conditions. Our model not

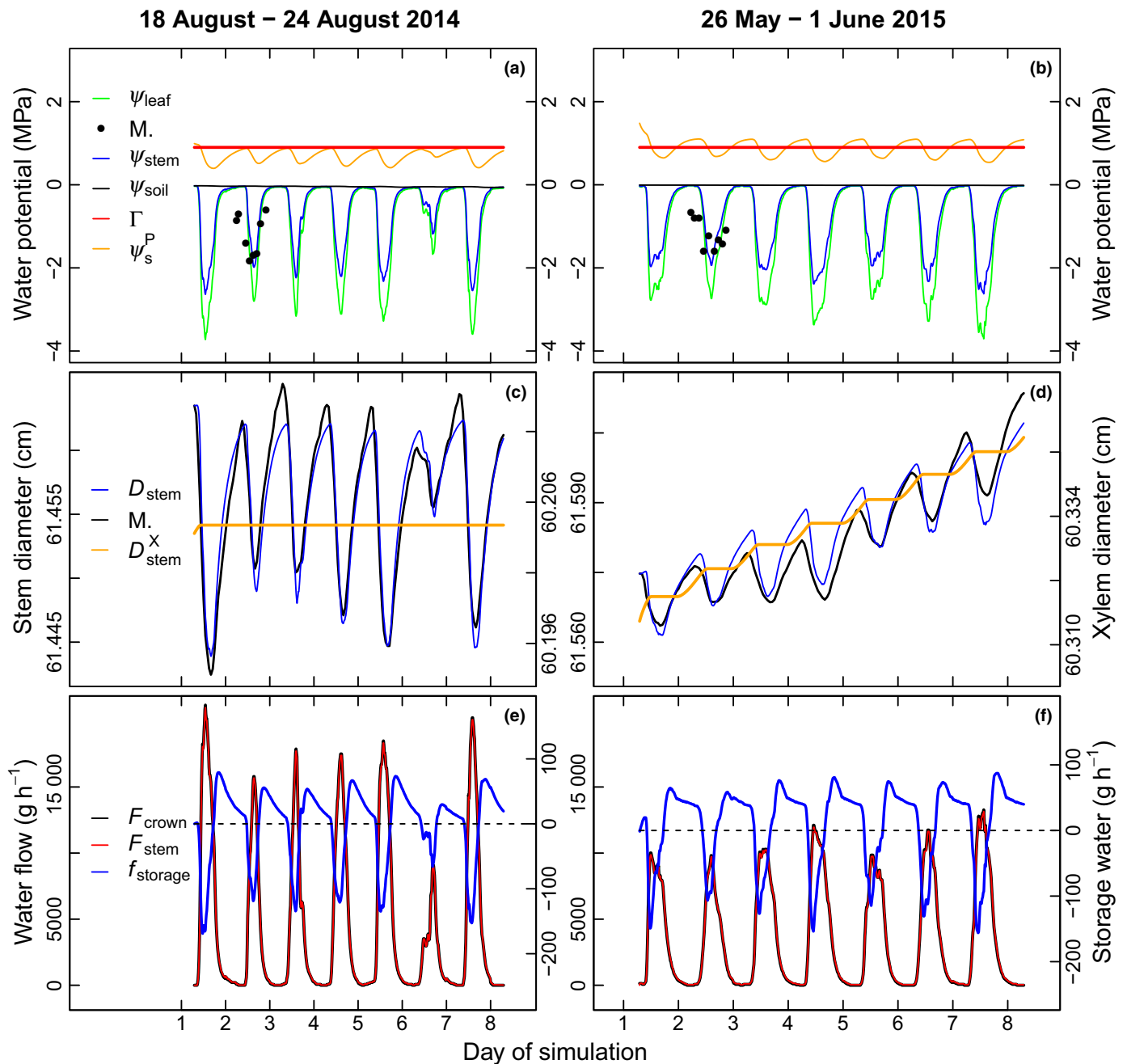


Fig. 3 One week of measured (M.) and simulated water potentials (a, b), diameter variations (c, d) and water flows (e, f) for *Picea abies* from the wet site at 1300 m (N13Wad_S2 in Table 1) during nongrowth (a, c, e) and growth (b, d, f) periods. Soil water potential (ψ_{soil} ; a, b) and sap flow (F_{crown} ; e, f) were used as model inputs, while leaf water potential (ψ_{leaf} ; a, b) and diameter variations (D_{stem} ; c, d) were measured. Growth of the xylem (D_{stem}^X ; xylem diameter axis; d) occurs during the night-time, when cell turgor pressure (ψ_s^P ; a, b) exceeds the critical value for wall-yielding (Γ). The flow of water to and from the storage compartment (f_{storage} ; storage water axis) affects the turgor pressure, which is defined by the mismatch between F_{crown} and direct stem water flow (F_{stem} ; e, f).

only supports the relevance of sink over source activity but also enabled us to identify threshold environmental conditions, a requested step for evolving the next generation of dynamic vegetation models – that is, those capable of appropriately representing wood formation processes in a tree’s stem (Babst *et al.*, 2018; Zuidema *et al.*, 2018). Our model illustrates that water and carbon are tightly interconnected in the tree, where turgor is at the

centre of this interaction and needs to be considered for simulating wood formation at daily to interannual resolutions.

The importance of turgor in explaining xylem growth

The turgor-driven growth model provided realistic wood formation estimates. Temporal dynamics of radial xylem growth rate

simulations showed agreement with xylogenesis observations (Fig. 4a), with maximum daily growth rates in June or July depending on site elevation. In addition, turgor-driven cell

enlargement processes can explain absolute ring-width patterns (Fig. 4b), which confirms the conceptual model presented by Cuny *et al.* (2014) and supports the importance of cell

Table 3 Statistic of stem diameter simulations (D_{stem} , mm) against dendrometer measurements for the 2015 calibration.

Site	Species	Tree	Slope	R^2	SSE	n
N13d	<i>Picea abies</i>	N13Ad_S1	0.98 ± 0.11	0.69 ± 0.15	0.30 ± 0.17	169
		N13Ad_S2	0.96 ± 0.05	0.95 ± 0.07	0.14 ± 0.12	
	<i>Larix decidua</i>	N13Bd_L1	1.02 ± 0.22	0.73 ± 0.14	0.45 ± 0.32	
N13w	<i>Larix decidua</i>	N13Bd_L2	0.99 ± 0.09	0.81 ± 0.10	0.33 ± 0.31	
		N13WAd_L1	1.05 ± 0.11	0.88 ± 0.08	0.06 ± 0.03	
		N13WBd_L2	0.99 ± 0.05	0.81 ± 0.18	0.35 ± 0.54	
	<i>Picea abies</i>	N13WBd_L3	1.01 ± 0.08	0.85 ± 0.09	0.31 ± 0.34	
		N13WAd_S1	0.99 ± 0.08	0.92 ± 0.11	0.14 ± 0.16	
		N13WAd_S2	1.00 ± 0.05	0.95 ± 0.04	0.14 ± 0.13	
S22	<i>Larix decidua</i>	N13WBd_S3	1.03 ± 0.06	0.90 ± 0.11	0.35 ± 0.32	
		S22Ad_L1	1.01 ± 0.09	0.82 ± 0.15	0.39 ± 0.60	
		S22Ad_L2	0.98 ± 0.14	0.80 ± 0.16	0.68 ± 0.81	

Overall mean of the slope of the linear relationships, goodness of fit (R^2), sum of squared errors (SSE) and sample size (n) are provided for all 7 d period calibrations performed per tree. Data are means \pm SD. The tree labels match labels presented in Table 1.

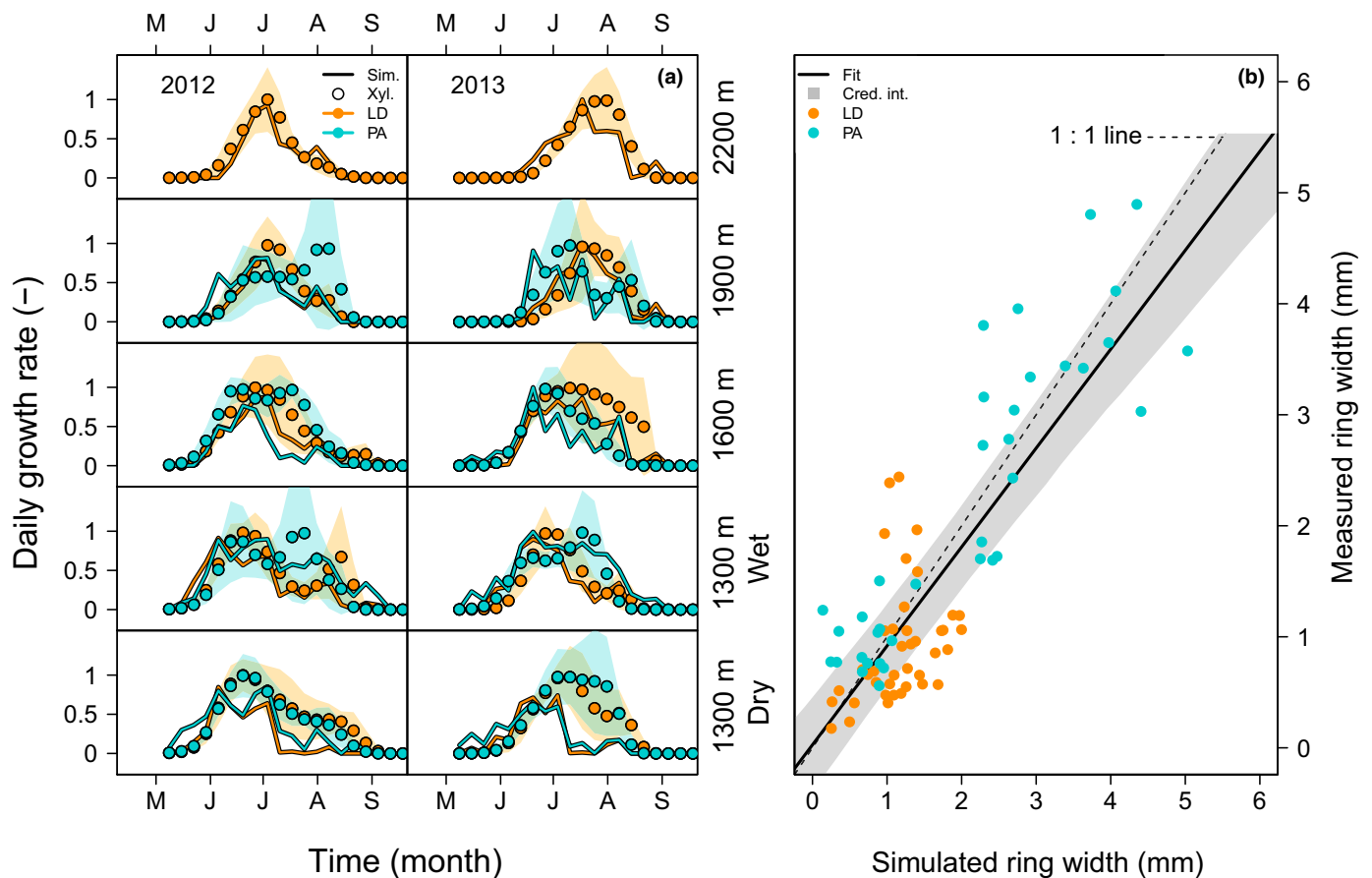


Fig. 4 Comparison between turgor-driven growth simulations and radial growth observations. (a) Xylogenesis-derived daily xylem growth rate (Xyl., shading indicates the standard deviation) against simulated values (Sim., coloured lines) for the 2012 and 2013 growing season. Data are averaged over all measured individuals per site and species (LD, *Larix decidua*; PA, *Picea abies*), and scaled to maximum daily growth rate for comparison. Note that no *P. abies* trees were monitored at 2200 m because of its limited occurrence at this elevation. (b) Simulated ring widths from 2012 to 2015 compared with observed ring widths from the increment cores of each individual tree per species. The solid line indicates a linear regression and the shaded area shows the Bayesian credible interval (Cred. int.) of the fitted function.

Table 4 Statistics for the linear relationship between xylogenesis-derived daily xylem growth rate and simulated values for the 2012 and 2013 growing seasons.

Site	Species	2012		2013			
		R^2	P	n	R^2	P	n
N13d	<i>Larix decidua</i>	0.47*	6.04e ⁻⁰⁴	21	0.21*	4.11e ⁻⁰²	20
	<i>Picea abies</i>	0.57*	1.14e ⁻⁰³	20	0.14*	1.11e ⁻⁰²	20
N13w	<i>Larix decidua</i>	0.55*	7.90e ⁻⁰⁵	22	0.72*	2.20e ⁻⁰⁶	20
	<i>Picea abies</i>	0.70*	3.98e ⁻⁰⁷	22	0.82*	8.63e ⁻⁰⁹	24
S16	<i>Larix decidua</i>	0.87*	7.28e ⁻¹¹	23	0.81*	1.15e ⁻⁰⁸	22
	<i>Picea abies</i>	0.54*	1.65e ⁻⁰⁴	21	0.57*	4.86e ⁻⁰⁵	22
S19	<i>Larix decidua</i>	0.83*	2.39e ⁻⁰⁸	20	0.86*	5.68e ⁻⁰⁹	20
	<i>Picea abies</i>	0.34*	5.32e ⁻⁰³	21	0.46*	1.03e ⁻⁰³	20
S22	<i>Larix decidua</i>	0.89*	1.68e ⁻⁰⁹	19	0.75*	1.98e ⁻⁰⁶	19

Linear-mixed effects models were used where the individual tree was incorporated as a random effect. Significant correlations are identified with an asterisk (*).

enlargement kinetics in defining the final dimensions of the wood structure. Finally, the validity of the simulated processes is supported by the fact that all calibrated parameters are realistic and within the range of previously reported values (see Notes S2, which also provides species-specific parameter values). The model shows a tendency to overestimate ring width (Fig. 4b), which could be as a result of xylem vs phloem cell production, which is currently considered a static process (f_{growth} , in Table S1) while it can change dynamically during the growing season (Prislan *et al.*, 2013). Additionally, the lower intra-annual performance observed at lower elevational sites, with drier conditions (≤ 1600 m asl; Fig. 4a) indicates the need to consider mechanisms that potentially maintain turgor pressure during drought (e.g. as found at the leaf level in Bartlett *et al.*, 2012). The current model uses a fixed initial osmotic potential (Π_s^i) and hence does not take into account dynamics in available sugars in the storage compartment. Phloem osmotic potential has been shown to increase with decreasing soil water potential, as a result of the mobilization of sugars (Lintunen *et al.*, 2016; Paljakka *et al.*, 2017), potentially increasing turgor pressure, thus demonstrating the relevance of considering nonstructural carbohydrate dynamics in the tree. Alternatively, discrepancies could be attributed to the uncertainty in xylogenesis measurements, indicated by the high standard deviation between trees used for wood formation monitoring (e.g. Fig. S10). Moreover, the intra-annual performance was generally lower for the evergreen *P. abies*, which could be related to a stronger carryover (or legacy) effect from previous years owing to the difference in leaf phenology (Zweifel & Sterck, 2018), which has not been specifically considered. This explanation is supported by the stronger dependency of ring width variability on temperature and precipitation from the previous year (Peters *et al.*, 2017).

Whereas we only considered sink activity (i.e. cambial activity and cell enlargement) and assumed carbon source to be not limiting, our mechanistic model showed appropriate performance. Yet, the variability in osmolality in the phloem (Paljakka *et al.*, 2017), including the dynamic regulation of sugar production (photosynthesis), transport, loading and unloading (De Schepper

& Steppe, 2010), could be highly relevant to further improving the model. For example, at the beginning and end of the growing period, the exchange resistance of water between xylem and phloem (R_s), followed by xylem sap flow resistance (R_x), is larger across sites and species (Fig. S9). This increase in R_s could be a result of seasonal dynamics in osmolality, where the concentration of nonstructural carbohydrates in the phloem is lower at the beginning and the end of the growing season, reducing both the flow of water to the storage compartment and the osmotic pressure (Simard *et al.*, 2013). Also, such R_s dynamics have been shown to be temperature-dependent (e.g. Steppe *et al.*, 2012). Alternative mechanisms have been hypothesized to drive the beginning and the end of growth. First, as incorporated in our model, cell wall extensibility is accelerated or decelerated, at high vs low temperatures, respectively, as a result of the enzymatic kinetics, which drive the release of cellulose microfibrils and could potentially halt growth at low temperatures (Cosgrove, 2000; Parent *et al.*, 2010). Second, hormonal signalling has been proposed, where lower auxin concentrations reduce growth at the beginning and end of the growing season (Steppe *et al.*, 2006, 2015; Hartmann *et al.*, 2017), forcing the modelled resistances for xylem and storage water transport (R_x and R_s , respectively) to increase, and reduce refilling of the storage compartment to increase turgidity. These hypotheses need to be further investigated to fully comprehend the mechanisms that halt growth and make our modelling approach suitable for predictive purposes. The increase in R_x , particularly at the end of the growing season, could also be induced by changes in physical properties of the xylem which could be induced by the occurrence of embolism as a result of drought (e.g. Steppe & Lemeur, 2007). Overall, our study validated a concrete approach for incorporating sink-limited growth processes such as turgor for multiple years in mature conifers. Our results provide evidence of the importance of turgor driving radial growth and a means to validate mechanistic models with independent weekly and annual growth observations.

Environmental regulation of turgor-driven growth and crown conductance

We found strong environmental control on turgor-driven growth. Our model allows turgor-driven growth limitation to be directly associated with corresponding environmental conditions, including atmospheric temperature (T_a) and soil water potential (ψ_{soil} ; Fig. 5). However, the existing collinearity among T_a , vapour pressure deficit and ψ_{soil} may be a result of interaction effects between them. The low probability of cell growth occurring below 2°C (23%; Fig. 5b) suggests a temperature threshold that is above the required photosynthetic minimum of *c.* 0°C (when assuming constant cell wall extensibility, ϕ ; Saxe *et al.*, 2001). However, our threshold lies below *c.* 5° C as determined by Körner (2008), which could be a result of the higher temporal resolution of our simulations. More critical is the observed halt of simulated growth at ψ_{soil} values < -0.6 MPa, which is less negative than ψ_{soil} constraining photosynthesis (Muller *et al.*, 2011) and suggests a strict control of growth by soil water availability for trees.

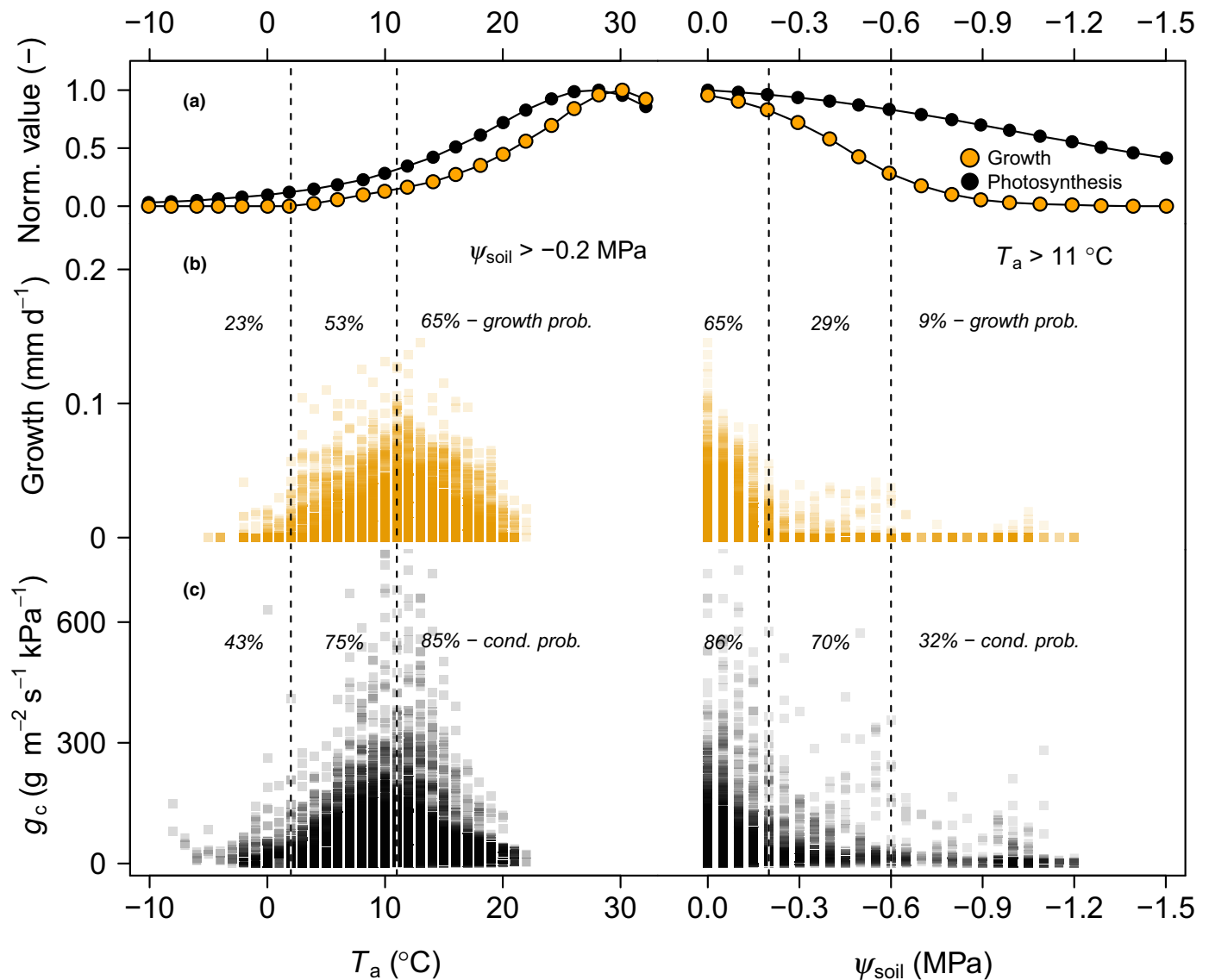


Fig. 5 Growth and crown conductance (g_c) responses to atmospheric temperature (T_a) and soil water potential (ψ_{soil}). (a) Response of sink (growth) and source (photosynthesis) activities to T_a and ψ_{soil} , reproduced from Faticchi *et al.* (2014). (b) Modelled radial growth rates (in mm d⁻¹) as a function of T_a (compiled in 1°C bins) and ψ_{soil} (compiled in 0.05 MPa bins) for all sites and species. For the T_a response, days with $\psi_{soil} < -0.2$ MPa were excluded, while for the ψ_{soil} response, days with a $T_a < 11^\circ\text{C}$ were excluded. (c) The same procedure was applied for daily mean g_c . Dotted lines indicate selected critical T_a and ψ_{soil} boundaries, for which we calculated the probability of growth ('growth prob.') and g_c ('cond. prob.'). These boundaries are presented to quantify the difference between growth and g_c in their environmental response. Growth and conductance probabilities are defined as the frequency of days with values above extremely low values ($> 2.5 \mu\text{m d}^{-1}$ for radial growth and $> 15 \text{ g m}^{-2} \text{ s}^{-1} \text{ kPa}^{-1}$ for g_c).

As stomatal conductance (expressed as crown conductance, g_c) is tightly linked to photosynthetic activity (Dewar *et al.*, 2018), we would expect that growth would start once water transport is initiated, in case growth is limited by the carbon source. When considering crown conductance derived from sap flow measurements (e.g. Meinzer *et al.*, 2013), we find a higher probability for trees to conduct water than to grow at temperatures below 2°C (Fig. 5c). These results suggest that photosynthesis starts at lower temperature than growth (Fig. 5a), although independent photosynthetic measurements are so far lacking. Interestingly, growth rates appear to decrease above 11°C , which disagrees with the apical meristem growth rates that decrease above *c.* 30°C (Fig. 5a; Parent *et al.*, 2010). This decrease above 11°C can be

explained by high vapour pressure deficit (D) at these temperatures, which prevents full refilling and subsequently induces lower turgidity (Fig. S12), which does not occur in controlled experimental setups (Parent *et al.*, 2010). We also find a steeper decrease with ψ_{soil} in daily growth rates than crown conductance (Fig. 5b,c). Yet, the low probability of growth between -0.2 and -0.6 MPa (29%) and almost no growth below -0.6 MPa (9%; Fig. 5b) indicates that higher D might have decreased stem water potential and caused a stronger inhibition of growth than what we would expect from decreasing ψ_{soil} alone (Muller *et al.*, 2011). When incorporating temperature dependence of enzymatic kinetics on ϕ , our simulations reveal that duration of turgor limitation becomes increasingly limited with increasing temperature during

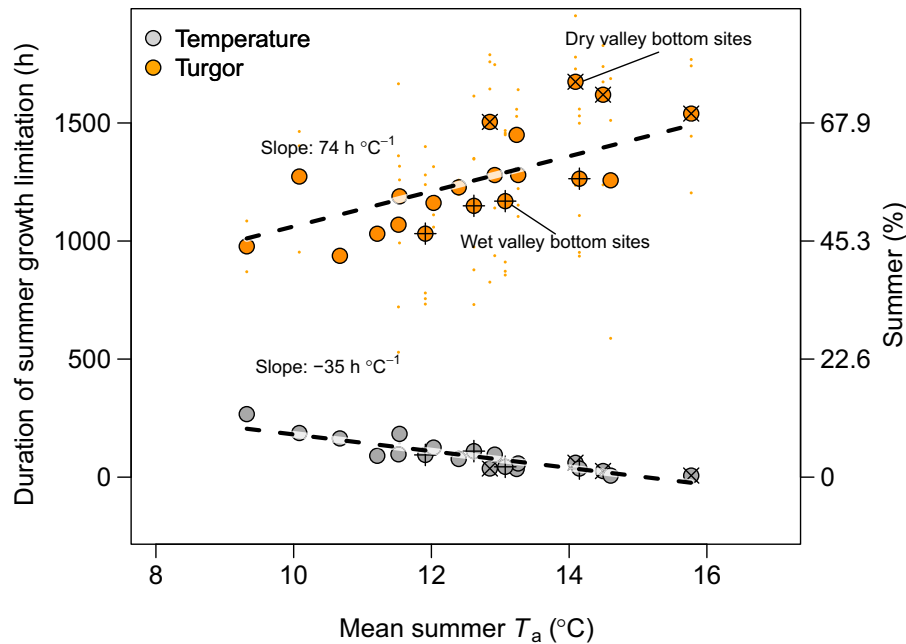


Fig. 6 Assessment of mean summer air temperature effect on growth duration by distinguishing between turgor- and temperature-dependent enzymatic constraints. Mean summer (June, July and August) atmospheric temperature (T_a) against the duration of growth limitation caused by temperature limitation (i.e. caused by cell wall extensibility (ϕ) regulated by temperature-dependent enzymatic kinetics; grey dots) and turgor limitation (i.e. turgor pressure (ψ_s^p) below the critical value for wall-yielding (I); orange dots). For each year the site mean of the duration of growth limitation was determined (large dots) from the individual specific simulations from 2012 to 2015 (small dots). The axis on the right indicates the duration of summer growth limitation as a percentage of the total summer period. The wet and dry sites at the valley bottom (1300 m asl) are highlighted with specified symbols. Significant linear relationships are indicated with a dashed line and the subsequent slope.

summer ($74 \text{ h } ^\circ\text{C}^{-1}$; Fig. 6) and the growing season ($147 \text{ h } ^\circ\text{C}^{-1}$), with the most severe limitation during soil droughts. Notably, this trend of increasing turgor limitation with increasing summer temperature is around two times stronger than the reduced temperature limitation affecting ϕ . The increase in turgor limitation could mechanistically explain why recent analyses show that tree growth becomes more limited by atmospheric water demand worldwide (Babst *et al.*, 2019).

Model limitations and implications

Models simulating wood formation vary in temporal scale and complexity, which has its inherent merits (Baert *et al.*, 2015; Friend *et al.*, 2019). Our presented model scales high in complexity and temporal resolution, where the use of moving-window calibration allows growth mechanisms to be disentangled and aids in establishing new hypotheses. However, this currently limits predictive capabilities and makes our approach most useful in terms of disentangling hydraulic signals in stem diameter variation from growth and defining environmental thresholds. Crucial steps have to be made to improve the model for predictive purposes in mature trees, such as advancing the understanding of dynamic behaviour of the calibrated parameters (e.g. C_{storage} , R_x , R_s or Π_s^i ; Salomón *et al.*, 2017). Hence, the measurements could be repeated at sites with continuously monitored photosynthetic activity to integrate water and carbon transport processes on a seasonal basis (De Schepper & Steppe, 2010; Mencuccini *et al.*, 2013; Steppe *et al.*, 2015). Additionally, to provide predictions

on the future fate of carbon stored within woody biomass (Cuny *et al.*, 2015), cell wall thickening and other process-based models that define wood anatomical structures could be considered (Vaganov *et al.*, 2006; Drew *et al.*, 2010; Steppe *et al.*, 2015). As the presented model considers overall radial wood formation, incorporating both cell enlargement and cell production, more detailed studies on these individual xylogenesis processes would be needed (e.g. Cabon *et al.*, 2020b). Notwithstanding, mechanistic modelling is crucial for constraining the environmental control on turgor dynamics and subsequently radial wood growth.

Our modelling efforts support the hypothesis that turgor is a critical factor in explaining sink limitation, which has implications for DGVMs. Specifically, our sites along a temperature gradient illustrate that increasing temperatures, and subsequent increases in vapour pressure deficit and soil drought, will significantly increase the duration of turgor-limiting growth, making this a key factor when considering the impact of global warming on forests. This increase in turgor limitation will be amplified with hotter droughts, although a better understanding is required of water-use strategies employed by tree species during drought. As turgidity is the engine of radial growth, this process should be considered in global models predicting future forest productivity (Hayat *et al.*, 2017). With the increasing efforts in detailed physiological data collection (Steppe *et al.*, 2016; Poyatos *et al.*, 2016; Chu *et al.*, 2017; Babst *et al.*, 2019) required to drive the mechanistic model presented in this study, the detection of environmental conditions when turgor is limiting growth becomes

feasible. This identification of key mechanisms and conditions under which environmental conditions are limiting growth should aid in further unravelling the source- vs sink-limited growth debate and improve the quality of vegetation model predictions regarding the future fate of forest carbon pools.

Acknowledgements

We thank Gregory King, Roger Köchli, Daniel Nievergelt, Kerstin Treydte and Anne Verstege for their aid in the extensive field and laboratory work. This work was funded by the Swiss National Science Foundation (SNSF) projects LOTFOR (grant 150205), CLIMWOOD (grant 160077), SNSF Early Postdoc.Mobility (grant P2BSP3_184475) and the COST Action network STReSS (grant FP1106). The authors declare there are no conflicts of interest.

Author contributions

RLP, PF, KS and DCF designed the study and performed the data collection. MS, HEC and CBKR contributed to data collection and processing. RLP and KS developed and applied the mechanistic model, with support from DJWDP and AC. RLP wrote the paper with support from all co-authors.

ORCID

Antoine Cabon  <https://orcid.org/0000-0001-6426-1726>
 Henri E. Cuny  <https://orcid.org/0000-0003-2098-5583>
 Patrick Fonti  <https://orcid.org/0000-0002-7070-3292>
 David C. Frank  <https://orcid.org/0000-0001-5463-5640>
 Richard L. Peters  <https://orcid.org/0000-0002-7441-1297>
 Cyrille B.K. Rathgeber  <https://orcid.org/0000-0001-7359-8320>
 Marcus Schaub  <https://orcid.org/0000-0002-0158-8892>
 Kathy Steppe  <https://orcid.org/0000-0001-6252-0704>

References

- Babst F, Bodesheim P, Charney N, Friend AD, Girardin MP, Klesse S, Moore DJP, Seftigen K, Björklund J, Bouriaud O *et al.* 2018. When tree rings go global: challenges and opportunities for retro- and prospective insight. *Quaternary Science Reviews* 197: 1–20.
- Babst F, Bouriaud O, Papale D, Gielen B, Janssens IA, Nikinmaa E, Ibrom A, Wu J, Bernhofer C, Köstner B *et al.* 2014. Above-ground woody carbon sequestration measured from tree rings is coherent with net ecosystem productivity at five eddy-covariance sites. *New Phytologist* 201: 1289–1303.
- Babst F, Bouriaud O, Poulter B, Trouet V, Girardin MP, Frank DC. 2019. Twentieth century redistribution in climatic drivers of global tree growth. *Science Advances* 5: 1–9.
- Baert A, De Schepper V, Steppe K. 2015. Variable hydraulic resistances and their impact on plant drought response modelling. *Tree Physiology* 35: 439–449.
- Bartlett MK, Scoffoni C, Sack L. 2012. The determinants of leaf turgor loss point and prediction of drought tolerance of species and biomes: a global meta-analysis. *Ecology Letters* 15: 393–405.
- Begg JE, Turner NC. 1970. Water potential gradients in field tobacco. *Plant Physiology* 46: 343–346.
- Boisvenue C, Running SW. 2006. Impacts of climate change on natural forest productivity – evidence since the middle of the 20th century. *Global Change Biology* 12: 862–882.
- Bonan GB. 2008. Forests and climate change: forcings, feedbacks, and the climate benefits of forests. *Science* 320: 1444–1449.
- Boyer JS. 1967. Leaf water potential measure with a pressure chamber. *Plant Physiology* 42: 133–137.
- Cabon A, Fernández-de-Uña L, Gea-Izquierdo G, Meinzer FC, Woodruff DR, Martínez-Vilalta J, De Cáceres M. 2020a. Water potential control of turgor-driven tracheid enlargement in Scots pine at its xeric distribution edge. *New Phytologist* 225: 209–221.
- Cabon A, Peters RL, Fonti P, Martínez-Vilalta J, De Cáceres M. 2020b. Temperature and water potential co-limit stem cambial activity along a steep elevational gradient. *New Phytologist* 226: 1325–1340.
- Chu H, Baldocchi DD, John R, Wolf S, Reichstein M. 2017. Fluxes all of the time? A primer on the temporal representativeness of FLUXNET. *Journal of Geophysical Research: Biogeosciences* 122: 289–307.
- Ciais P, Reichstein M, Viovy N, Granier A, Ogée J, Allard V, Aubinet M, Buchmann N, Bernhofer C, Carrara A *et al.* 2005. Europe-wide reduction in primary productivity caused by the heat and drought in 2003. *Nature* 437: 529–533.
- Cosgrove D. 1986. Biophysical control of plant cell growth. *Annual Review of Plant Physiology* 37: 377–405.
- Cosgrove DJ. 2000. Loosening of plant cell walls by expansins. *Nature* 407: 321–326.
- Cox PM, Betts RA, Jones CD, Spall SA, Totterdell IJ. 2000. Acceleration of global warming due to carbon-cycle feedbacks in a coupled climate model. *Nature* 408: 184–187.
- Cuny HE, Fonti P, Rathgeber CBK, von Arx G, Peters RL, Frank DC. 2019. Couplings in cell differentiation kinetics mitigate air temperature influence on conifer wood anatomy. *Plant, Cell & Environment* 42: 1222–1232.
- Cuny HE, Rathgeber CBK. 2016. Xylogenesis: Coniferous trees of temperate forests are listening to the climate tale during the growing season but only remember the last words!. *Plant Physiology* 171: 306–317.
- Cuny HE, Rathgeber CBK, Frank D, Fonti P, Fournier M. 2014. Kinetics of tracheid development explain conifer tree-ring structure. *New Phytologist* 203: 1231–1241.
- Cuny HE, Rathgeber CBK, Frank D, Fonti P, Mäkinen H, Prislán P, Rossi S, Martínez del Castillo E, Campelo F, Vavřík H *et al.* 2015. Woody biomass production lags stem-girth increase by over one month in coniferous forests. *Nature Plants* 1: 1–6.
- De Kauwe MG, Medlyn BE, Zaehle S, Walker AP, Dietze MC, Wang YP, Luo Y, Jain AK, El-Masri B, Hickler T *et al.* 2014. Where does the carbon go? A model-data intercomparison of vegetation carbon allocation and turnover processes at two temperate forest free-air CO₂ enrichment sites. *New Phytologist* 203: 883–899.
- De Schepper V, Steppe K. 2010. Development and verification of a water and sugar transport model using measured stem diameter variations. *Journal of Experimental Botany* 61: 2083–2099.
- De Swaef T, Steppe K. 2010. Linking stem diameter variations to sap flow, turgor and water potential in tomato. *Functional Plant Biology* 37: 429–438.
- Delpierre N, Berveiller D, Granda E, Dufrene E. 2016. Wood phenology, not carbon input, controls the interannual variability of wood growth in a temperate oak forest. *New Phytologist* 210: 459–470.
- Dewar R, Mauranen A, Mäkelä A, Hölttä T, Medlyn B, Vesala T. 2018. New insights into the covariation of stomatal, mesophyll and hydraulic conductances from optimization models incorporating nonstomatal limitations to photosynthesis. *New Phytologist* 217: 571–585.
- Drew DM, Downes GM, Battaglia M. 2010. CAMBIUM, a process-based model of daily xylem development in *Eucalyptus*. *Journal of Theoretical Biology* 264: 395–406.
- Eyring H. 2004. The activated complex in chemical reactions. *The Journal of Chemical Physics* 3: 107–115.
- Fatichi S, Leuzinger S, Körner C. 2014. Moving beyond photosynthesis: from carbon source to sink-driven vegetation modelling. *New Phytologist* 201: 1086–1095.

- Fatichi S, Pappas C, Zscheischler J, Leuzinger S. 2019. Modelling carbon sources and sinks in terrestrial vegetation. *New Phytologist* 221: 652–668.
- Fonti P, Jansen S. 2012. Xylem plasticity in response to climate. *New Phytologist* 195: 734–736.
- Fournier M, Stokes A, Coutand C, Fourcaud T, Mouliat B. 2006. Tree biomechanics and growth strategies in the context of forest functional ecology. In: Herrel A, Speck T, Rowe NP, eds. *Ecology and biomechanics: a mechanical approach to the ecology of animals and plants*. Boca Raton, FL, USA: CRC Press, 1–33.
- Friend AD, Patrick AHE, Tim F, Rathgeber CBK, Richardson AD, Turton RH. 2019. On the need to consider wood formation processes in global vegetation models and a suggested approach. *Annals of Forest Science* 76: 49.
- Génard M, Dauzat J, Franck N, Lescourret F, Moitrier N, Vaast P, Vercambre G. 2008. Carbon allocation in fruit trees: From theory to modelling. *Trees* 22: 269–282.
- Génard M, Fishman S, Vercambre G, Hugué J-G, Bussi C, Besset J, Habib R. 2001. A biophysical analysis of stem and root diameter variations in woody plants. *Plant Physiology* 126: 188–202.
- Grossiord C, Grossiord C, Buckley TN, Cernusak LA, Novick KA, Poulter B, Siegwolf RTW, Sperry JS, McDowell NG. 2020. Plant responses to rising vapor pressure deficit. *New Phytologist* 226: 1550–1566.
- Guillemot J, Francois C, Hmimina G, Dufrière E, Martin-StPaul NK, Soudani K, Marie G, Ourcival JM, Delpierre N. 2017. Environmental control of carbon allocation matters for modelling forest growth. *New Phytologist* 214: 180–193.
- Hartmann F, Rathgeber C, Fournier M, Mouliat B. 2017. Modelling wood formation and structure: power and limits of a morphogenetic gradient in controlling xylem cell proliferation and growth. *Annals of Forest Science* 74: 1–15.
- Hayat A, Hackett-pain AJ, Pretzsch H, Rademacher TT, Friend AD. 2017. Modeling tree growth taking into account carbon source and sink limitations. *Frontiers in Plant Science* 8: 1–15.
- Hölttä T, Mäkinen H, Nöjd P, Mäkelä A, Nikinmaa E. 2010. A physiological model of softwood cambial growth. *Tree Physiology* 30: 1235–1252.
- Huntzinger DN, Michalak AM, Schwalm C, Ciais P, King AW, Fang Y, Schaefer K, Wei Y, Cook RB, Fisher JB *et al.* 2017. Uncertainty in the response of terrestrial carbon sink to environmental drivers undermines carbon-climate feedback predictions. *Scientific Reports* 7: 1–8.
- Johnson FH, Eyring H, Williams RW. 1942. The nature of enzyme inhibitions in bacterial luminescence: Sulfanilamide, urethane, temperature and pressure. *Journal of Cellular and Comparative Physiology* 20: 247–268.
- King G, Fonti P, Nievergelt D, Büntgen U, Frank D. 2013. Climatic drivers of hourly to yearly tree radius variations along a 6°C natural warming gradient. *Agricultural and Forest Meteorology* 168: 36–46.
- Klesse S, Babst F, Lienert S, Spahni R, Joos F, Bouriaud O, Carrer M, Di Filippo A, Poulter B, Trotsiuk V *et al.* 2018. A combined tree-ring and vegetation model assessment of European forest growth sensitivity to inter-annual climate variability. *Global Biogeochemical Cycles* 32: 1226–1240.
- Körner C. 2003. Carbon limitation in trees. *Journal of Ecology* 91: 4–17.
- Körner C. 2008. Winter crop growth at low temperature may hold the answer for alpine treeline formation. *Plant Ecology & Diversity* 1: 3–11.
- Kozłowski TT, Pallardy SG. 1997. *Physiology of woody plants*. San Diego, CA, USA: Academic Press.
- Leuzinger S, Manusch C, Bugmann H, Wolf A. 2013. A sink-limited growth model improves biomass estimation along boreal and alpine tree lines. *Global Ecology and Biogeography* 22: 924–932.
- Lintunen A, Paljakka T, Jyske T, Peltoniemi M, Sterck F, von Arx G, Cochard H, Copini P, Caldeira MC, Delzon S *et al.* 2016. Osmolality and non-structural carbohydrate composition in the secondary phloem of trees across a latitudinal gradient in Europe. *Frontiers in Plant Science* 7: 1–15.
- Lockhart JA. 1965. An analysis of irreversible plant cell elongation. *Journal of Theoretical Biology* 8: 264–275.
- Meinzer FC, Woodruff DR, Eissenstat DM, Lin HS, Adams TS, McCulloh KA. 2013. Above- and belowground controls on water use by trees of different wood types in an eastern US deciduous forest. *Tree Physiology* 33: 345–356.
- Mencuccini M, Hölttä T, Sevanto S, Nikinmaa E. 2013. Concurrent measurements of change in the bark and xylem diameters of trees reveal a phloem-generated turgor signal. *New Phytologist* 198: 1143–1154.
- Mencuccini M, Salmon Y, Mitchell P, Hölttä T, Choat B, Meir P, O'Grady A, Tissue D, Zweifel R, Sevanto S *et al.* 2017. An empirical method that separates irreversible stem radial growth from bark water content changes in trees: theory and case studies. *Plant, Cell & Environment* 40: 290–303.
- Moser L, Fonti P, Büntgen U, Esper J, Luterbacher J, Franzen J, Frank D. 2009. Timing and duration of European larch growing season along altitudinal gradients in the Swiss Alps. *Tree Physiology* 30: 225–233.
- Muller B, Pantin F, Génard M, Turc O, Freixes S, Piques M, Gibon Y. 2011. Water deficits uncouple growth from photosynthesis, increase C content, and modify the relationships between C and growth in sink organs. *Journal of Experimental Botany* 62: 1715–1729.
- Nikinmaa E, Sievanen R, Hölttä T. 2014. Dynamics of leaf gas exchange, xylem and phloem transport, water potential and carbohydrate concentration in a realistic 3-D model tree crown. *Annals of Botany* 114: 653–666.
- Norby RJ, Warren JM, Iversen CM, Medlyn BE, McMurtrie RE. 2010. CO₂ enhancement of forest productivity constrained by limited nitrogen availability. *Proceedings of the National Academy of Sciences, USA* 107: 19368–19373.
- Paljakka T, Jyske T, Lintunen A, Aaltonen H, Nikinmaa E, Hölttä T. 2017. Gradients and dynamics of inner bark and needle osmotic potentials in Scots pine (*Pinus sylvestris* L.) and Norway spruce (*Picea abies* L. Karst). *Plant, Cell & Environment* 40: 2160–2173.
- Pan Y, Birdsey RA, Fang J, Houghton R, Kauppi PE, Kurz WA, Phillips OL, Shvidenko A, Lewis SL, Canadell JG *et al.* 2011. A large and persistent carbon sink in the world's forests. *Science* 333: 988–994.
- Pappas C, Maillet J, Rakowski S, Baltzer JL, Barr AG, Black TA, Fatichi S, Laroque CP, Matheny AM, Roy A *et al.* 2020. Aboveground tree growth is a minor and decoupled fraction of boreal forest carbon input. *Agricultural and Forest Meteorology* 290: 108030.
- Parent B, Tardieu F. 2012. Temperature responses of developmental processes have not been affected by breeding in different ecological areas for 17 crop species. *New Phytologist* 194: 760–774.
- Parent B, Turc O, Gibon Y, Stitt M, Tardieu F. 2010. Modelling temperature-compensated physiological rates, based on the co-ordination of responses to temperature of developmental processes. *Journal of Experimental Botany* 61: 2057–2069.
- Peters RL, Balanzategui D, Hurley AG, von Arx G, Prendin AL, Cuny HE, Björklund J, Frank DC, Fonti P. 2018. RAPTOR: row and position tracheid organizer in R. *Dendrochronologia* 47: 10–16.
- Peters RL, Fonti P, Frank DC, Poyatos R, Pappas C, Kahmen A, Carraro V, Prendin AL, Schneider L, Baltzer JL *et al.* 2018. Quantification of uncertainties in conifer sap flow measured with the thermal dissipation method. *New Phytologist* 219: 1283–1299.
- Peters RL, Klesse S, Fonti P, Frank DC. 2017. Contribution of climate vs. larch budmoth outbreaks in regulating biomass accumulation in high-elevation forests. *Forest Ecology and Management* 401: 147–158.
- Peters RL, Speich M, Pappas C, Kahmen A, von Arx G, Graf Pannatier E, Steppe K, Treyde K, Stritih A, Fonti P. 2019. Contrasting stomatal sensitivity to temperature and soil drought in mature alpine conifers. *Plant, Cell & Environment* 42: 1674–1689.
- Pinheiro J, Bates D, DebRoy S, Sarkar D, R Core Team. 2020. *Nlme: linear and nonlinear mixed effects models. R package v.3.1-144*. [WWW document] URL <https://CRAN.R-project.org/package=nlme>.
- Popkin G. 2019. How much can forests fight climate change? *Nature* 565: 280–282.
- Poyatos R, Granda V, Molowny-horas R, Mencuccini M, Steppe K, Martínez-vilalta J. 2016. SAPFLUXNET: Towards a global database of sap flow measurements. *Tree Physiology* 36: 1449–1455.
- Prislan P, Gričar J, de Luis M, Smith KT, Čufar K. 2013. Phenological variation in xylem and phloem formation in *Fagus sylvatica* from two contrasting sites. *Agricultural and Forest Meteorology* 180: 142–151.
- Pugh TAM, Müller C, Arneth A, Haverd V, Smith B. 2016. Key knowledge and data gaps in modelling the influence of CO₂ concentration on the terrestrial carbon sink. *Journal of Plant Physiology* 203: 3–15.
- R Core Team. 2013. *R: A language and environment for statistical computing*. Vienna, Austria: R Foundation for Statistical Computing. [WWW document] URL <https://www.R-project.org/>

- Rathgeber CBK, Cuny HE, Fonti P. 2016. Biological basis of tree-ring formation: a crash course. *Frontiers in Plant Science* 7: 1–7.
- Rossi S, Anfodillo T, Cufar K, Cuny HE, Deslauriers A, Fonti P, Frank D, Gričar J, Gruber A, Huang JG *et al.* 2016. Pattern of xylem phenology in conifers of cold ecosystems at the Northern Hemisphere. *Global Change Biology* 22: 3804–3813.
- Salomón RL, De Roo L, Oleksyn J, De Pauw DJW, Steppe K. 2019. TReSpire – a biophysical TRee Stem respiration model. *New Phytologist* 225: 2214–2230.
- Salomón RL, Limousin J-M, Ourcival J-M, Rodríguez-Calcerrada J, Steppe K. 2017. Stem hydraulic capacitance decreases with drought stress: implications for modelling tree hydraulics in the Mediterranean oak *Quercus ilex*. *Plant, Cell & Environment* 40: 1379–1391.
- Saxe H, Cannell MGR, Johnsen Ø, Ryan MG, Vourlitis G. 2001. Tree and forest functioning in response to global warming. *New Phytologist* 149: 369–400.
- Simard S, Giovannelli A, Treydte K, Traversi ML, King GM, Frank D, Fonti P. 2013. Intra-annual dynamics of non-structural carbohydrates in the cambium of mature conifer trees reflects radial growth demands. *Tree Physiology* 33: 913–923.
- Sitch S, Huntingford C, Gedney N, Levy PE, Lomas M, Piao SL, Betts R, Ciais P, Cox P, Friedlingstein P *et al.* 2008. Evaluation of the terrestrial carbon cycle, future plant geography and climate-carbon cycle feedbacks using five Dynamic Global Vegetation Models (DGVMs). *Global Change Biology* 14: 2015–2039.
- Steppe K, Cochard H, Lacoite A, Améglio T. 2012. Could rapid diameter changes be facilitated by a variable hydraulic conductance? *Plant, Cell & Environment* 35: 150–157.
- Steppe K, De Pauw DJW, Lemeur R, Vanrolleghem A. 2006. A mathematical model linking tree sap flow dynamics to daily stem diameter fluctuations and radial stem growth. *Tree Physiology* 26: 257–273.
- Steppe K, Lemeur R. 2007. Effects of ring-porous and diffuse-porous stem wood anatomy on the hydraulic parameters used in a water flow and storage model. *Tree Physiology* 27: 43–52.
- Steppe K, Sterck F, Deslauriers A. 2015. Diel growth dynamics in tree stems: linking anatomy and ecophysiology. *Trends in Plant Science* 20: 335–343.
- Steppe K, von der Crone J, De Pauw DJW. 2016. TreeWatch.net: a tree water and carbon monitoring network to assess instant tree hydraulic functioning and stem growth. *Frontiers Plant Science* 7: 993.
- Tardieu F, Granier C, Muller B. 2011. Water deficit and growth. Co-ordinating processes without an orchestrator? *Current Opinion in Plant Biology* 14: 283–289.
- Tei S, Sugimoto A, Yonenobu H, Matsuura Y, Osawa A, Sato H, Fujinuma J, Maximov T. 2017. Tree-ring analysis and modelling approaches yield contrary response of circumboreal forest productivity to climate change. *Global Change Biology* 23: 5179–5188.
- Vaganov EA, Hughes MK, Shashkin AV. 2006. *Growth dynamics of conifer tree rings: images of past and future environments*. Berlin, Germany: Springer-Verlag.
- Von Arx G, Carrer M. 2014. Roxas – a new tool to build centuries-long tracheid-lumen chronologies in conifers. *Dendrochronologia* 32: 290–293.
- WMO. 2008. *Guide to meteorological instruments and methods of observation, appendix 4B, WMO-No. 8 (CI-MO guide)*. Geneva, Switzerland: World Meteorological Organization.
- Zuidema PA, Poulter B, Frank DC. 2018. A wood biology agenda to support global vegetation modelling. *Trends in Plant Science* 23: 1006–1015.
- Zweifel R, Sterck F. 2018. A conceptual tree model explaining legacy effects on stem growth. *Frontiers in Forests and Global Change* 1: 1–9.

Supporting Information

Additional Supporting Information may be found online in the Supporting Information section at the end of the article.

Fig. S1 Diagram providing the mean monthly air temperature measured at the sites and the monthly precipitation.

Fig. S2 Species-specific relationship between diameter at breast height (DBH) and phloem thickness (T_{phloem}).

Fig. S3 Species-specific relationship between branch (Ψ_{leaf}) and stem water potential (Ψ_{stem}).

Fig. S4 Xylem growth fraction (f_{growth}) for three species obtained from the literature.

Fig. S5 Comparison between predawn branch water potential (Ψ_{leaf}) from *Picea abies* and *Larix decidua* and soil water potential (Ψ_{soil}).

Fig. S6 Example of a sensitivity analysis for *Picea abies* at N13w during nongrowth and growth periods.

Fig. S7 Boxplots of differences in model performance when fixing parameters.

Fig. S8 Boxplots of 2015 weekly calibrated parameters grouped per site and species and effect of parameter fixing on model performance.

Fig. S9 Example of a 7 d moving-window calibration with an overlap of 3 d for the growing season of 2012 for a *Larix decidua* tree.

Fig. S10 Daily growth rates for all sites and species for which xylogenesis observations have been performed in 2012 and 2013.

Fig. S11 Calibrated flow resistance in the stem compartment of the active xylem (R_x) and exchange resistance between the active xylem of the stem and the storage compartment (R_s) from the four growing season calibrations.

Fig. S12 Simulated growth rates against vapour pressure deficit (D) for both *Picea abies* and *Larix decidua* and the relationship between D and atmospheric temperature (T_a) for all sites.

Note S1 Model calibration and sensitivity and identifiability analysis.

Note S2 Model performance when constraining hydraulic capacitance of the storage tissue (C_{storage}) or hydraulic resistance of the stem (R_x).

Table S1 Overview of model parameters.

Table S2 Overview of sites sampled for phloem thickness allometric relationships.

Table S3 Summary statistics of linear mixed-effects model applied on diameter at breast height (DBH) versus phloem thickness (T_{phloem}).

Table S4 Summary statistics of linear mixed-effects model applied on branch water potential (Ψ_{leaf}) vs stem water potential (Ψ_{stem}).

Table S5 Mean and standard deviation of the model parameters for individual trees and averaged per species obtained from the weekly calibrations during the growing season of 2015.

Table S6 Overview of the species' average of hydraulic capacitance of the storage tissue (C_{storage}) and hydraulic resistance of the stem (R_x) reported in the literature.

Please note: Wiley Blackwell are not responsible for the content or functionality of any Supporting Information supplied by the authors. Any queries (other than missing material) should be directed to the *New Phytologist* Central Office.



About *New Phytologist*

- *New Phytologist* is an electronic (online-only) journal owned by the New Phytologist Foundation, a **not-for-profit organization** dedicated to the promotion of plant science, facilitating projects from symposia to free access for our Tansley reviews and Tansley insights.
- Regular papers, Letters, Research reviews, Rapid reports and both Modelling/Theory and Methods papers are encouraged. We are committed to rapid processing, from online submission through to publication 'as ready' via *Early View* – our average time to decision is <26 days. There are **no page or colour charges** and a PDF version will be provided for each article.
- The journal is available online at Wiley Online Library. Visit **www.newphytologist.com** to search the articles and register for table of contents email alerts.
- If you have any questions, do get in touch with Central Office (np-centraloffice@lancaster.ac.uk) or, if it is more convenient, our USA Office (np-usaoffice@lancaster.ac.uk)
- For submission instructions, subscription and all the latest information visit **www.newphytologist.com**